Article

Polarimetric ALOS PALSAR Time Series in Mapping Biomass of Boreal Forests

Oleg Antropov [1],*, Yrjö Rauste [2], Tuomas Häme [2] and Jaan Praks [1]

[1] Department of Electronics and Nanoengineering, School of Electrical Engineering, Aalto University, P.O. Box 11000, FI-00076 AALTO, 02150 Espoo, Finland; jaan.praks@aalto.fi

[2] VTT Technical Research Centre of Finland Ltd., Remote Sensing Team, PL 1000, FI-02044 VTT Espoo, Finland; yrjo.rauste@vtt.fi (Y.R.); tuomas.hame@vtt.fi (T.H.)

* Correspondence: oleg.antropov@aalto.fi

Abstract: Here, we examined multitemporal behavior of fully polarimetric SAR (PolSAR) parameters at L-band in relation to the stem volume of boreal forests. The PolSAR parameters were evaluated in terms of their temporal consistency, inter-dependence and suitability for forest stem volume estimation across several seasonal conditions (frozen, thaw and unfrozen). The satellite SAR data were represented by a time series of PolSAR images acquired during several seasons in the years 2006 to 2009 by the ALOS PALSAR sensor. The study area was in central Finland, and represented a managed area in typical boreal mixed forest land. Utility of different PolSAR parameters, their temporal stability and cross-correlations were studied along with reference stand-level stem volume data from forest inventory. Further, two polarimetric parameters, cross-polarization backscatter and co-polarization coherence, were chosen for further investigation and stem volume retrieval. A relationship between forest stem volume and PolSAR parameters was established using the kNN regression approach. Ways of optimally combining PolSAR images were evaluated as well. For a single scene, best results were observed with polarimetric coherence (RMSE ≈ 38.8 m³/ha) for scene acquired in frozen conditions. An RMSE of 40.8 m³/ha (42.9%, $R^2 = 0.66$) was achieved for cross-polarization backscatter in the best case. Cross-polarization backscatter was a better predictor than polarimetric coherence for few summer scenes. Multitemporal aggregation of selected PolSAR scenes improved estimates for both studied PolSAR parameters. Stronger improvement was observed for coherence with RMSE down to 34 m³/ha (35.8%, $R^2 = 0.77$) compared to 38.8–51.6 m³/ha (40.8–54.3%) from separate scenes. Finally, the accuracy statistics reached RMSE of 32.2 m³/ha (34%, $R^2 = 0.79$) when multitemporal HHVV coherence was combined with multitemporal HV-backscatter.

Keywords: synthetic aperture radar; SAR polarimetry; time series; stem volume; boreal forest; L-band; ALOS PALSAR

1. Introduction

Aboveground biomass (AGB) is a key biophysical ecosystem variable describing all living biomass above the soil including stem, stump, branches, bark, seeds and foliage [1]. Cost-effective assessment and monitoring of forest biomass is central for effective forest industry, resource planning and sustainable forest management [2]. Forest biomass has been recognized as a terrestrial Essential Climate Variable [3], and its importance in global terms has become even greater in recent years due to international concerns about climate warming [2,4].

Remote sensing of forest structure and biomass with synthetic aperture radar (SAR) bears significant potential for mapping and understanding forest ecological processes [5–7]. These techniques could serve as valuable methods for biomass assessment of heterogeneous complex

biophysical environments. Special interest is to multiparametric SAR data for forest properties assessment and monitoring. Polarimetric SAR (PolSAR) could be a suitable alternative with active development particularly in forestry applications [8]. Further, we will use the term PolSAR exclusively for quad-polarimetric SAR, in contrast to, e.g., dual-polarization SAR.

Saturation of the radar-biomass relationship at higher levels of forest biomass is a well-known difficulty of SAR-based mapping of AGB [9,10]. Due to greater sensitivity to the woody components and higher penetration through forest canopy at a longer wavelength, L- and P-band SAR data are considered more suitable for forest stem volume retrieval, compared to SAR data acquired at higher microwave frequencies. Among established and newly developed imaging configurations and techniques utilizing SAR imagery in forest characterization, such as multitemporal, polarimetric, multifrequency, interferometric, polarimetric-interferometric and tomographic SAR, only the first two are presently routinely available at L-band from space.

In this study, we will concentrate on fully polarimetric and multitemporal SAR, merging these techniques to investigate multitemporal behavior of PolSAR images and synergy it might offer for advanced forest variable assessment. As the forest inventory measurements are represented by stand level measurements of forest stem volume, which in the case of boreal forest can be recalculated to AGB using simple factors [11], the terms AGB, forest biomass and forest stem volume are used further interchangeably in this paper.

Polarimetric SAR signatures are sensitive to individual particle characteristics dictated by particle geometry (such as particle orientations and shapes) and dielectric constants (thus effectively moisture content), as well as ensemble average entropy [12,13]. Furthermore, incoherent model-based PolSAR decompositions permit separating main scattering contributions from vegetated areas, which consist of surface, even-bounce, and volume scattering [14]. However, as the number of independent polarimetric observables is limited to nine (in monostatic backscattering case), only relatively simple scattering mechanism models can be employed for the identification and separation of corresponding contributions. For surface and double-bounce scattering, typically first-order models are used, whereas modeling of scattering from vegetation has achieved more focus in recent literature [14–16]. Additionally, different ratios [17] and correlations based on the second order statistics of SAR data are often used to establish empirical or semi-empirical relationships between PolSAR observables and forest variables [18–20], in PolSAR based forest classification [21,22] and land cover mapping [23,24].

Polarimetric SAR research with airborne instruments has been active since early days of SAR polarimetry. Several studies were made particularly with airborne PolSAR data at P-, L- and C-bands aiming at forest parameter estimation and AGB retrieval. Forest biomass retrieval was attempted with polarization phase difference [10], followed by incorporating polarimetric coherence [25]. Radar backscatter intensities and polarimetric coherence were useful in improving forest biomass estimation with simple regression model [26] in boreal forest. Polarization phase difference and coherence were used for the retrieval of biomass in mangroves forest, with the polarimetric coherence exhibiting a clear sensitivity to forest biomass [27]. Useful features of polarimetric coherence were studied in [28] further relating it to diverse forest types and biomass classes. In [29], a linear correlation of polarimetric anisotropy to tree height up till 25 m was observed, while alpha angle and entropy saturated at much lower tree heights. In [30], airborne L-band SAR data were used to study polarization phase difference, polarimetric coherence and the volume scattering component of the Freeman-Durden decomposition [14] (that is cross-polarization backscatter) in multiple regression over tropical forest. Comparable results were achieved in [31] over boreal forest, where averaged scattering mechanism and cross-polarization intensity were found to be best correlated with forest stem volume. Further, polarization synthesis was used to improve correlations between PolSAR data and forest variables [32–34].

The opportunity to use multi-polarization (including quad-polarimetric) and multitemporal SAR data at L-band was offered by a Phased Array type L-band Synthetic Aperture Radar (PALSAR) sensor on-board ALOS during its life span of more than five years [35], followed by its successor ALOS-2 PALSAR-2. As fully polarimetric satellite SAR data were collected by PALSAR only and

were not routinely available for wide area forest mapping [11,36,37], only few studies are known aiming at the assessment of forest properties with quad-pol PALSAR. However, in the view of ALOS PALSAR-2 mission and other potential L-band missions, development of effective methodologies for retrieving forest parameters from PolSAR L-land data are timely and necessary.

Due to earlier L-band spaceborne imaging radars operating in a single-polarization imaging mode, not many papers are available for objective comparison using multi-polarization capability, particularly in the boreal forest. Few recent studies [38–42] indicate a potential of the ALOS PALSAR data for stand-wise stem volume retrieval in the boreal forest zone, noting seasonal and multitemporal dependence of estimates. However, the problem is that approaches demonstrated so far with spaceborne SAR data at L-band gave satisfactory results only when produced biomass estimates were aggregated to relatively large areas [41]. Another problem is suboptimal inversion scenario in model-based approaches, which may complicate routine stem volume estimation due to non-physical, negative or unrealistically high estimates of AGB, as discussed in [39]. Chowdhury et al. used PolSAR variables in linear regression fitting [43] and polarimetric coherence in semi-empirical model inversion [42] to recover growing stock volume of Siberian forests. Results were encouraging with up to 33 m³/ha RMSE. However, the reference data were relatively outdated and stand sizes were relatively big with large variation in size. As the forest was mostly natural, it is interesting to study respective dependencies over managed forest areas with smaller stands. Another reason is that fully polarimetric ALOS PALSAR data were used in the fitting against reference data mostly on scene by scene basis (in contrast to single- and dual-pol ALOS PALSAR studies notably in [44]). Multitemporal behavior of PolSAR parameters was not analyzed in-depth, aside from cross-correlation check-ups in [42]. In addition, models employed rely primarily on WCM-based or simple regression fitting, while more advanced computational approaches were not studied. To date, comprehensive quad-pol ALOS PALSAR time series were rarely collected and available only over selected areas.

In this study, for the first time fully polarimetric spaceborne L-band SAR data were combined using suitable PolSAR parameters, for forest stem volume estimation. The focus of this study was two-fold. Firstly, we examined multitemporal behavior of several PolSAR parameters suitable for forest biomass mapping, particularly covering aforementioned gaps. Understanding their cross-correlation and temporal dynamics across several seasons can help identify more stable PolSAR parameters for their optimal aggregation and substitution. Secondly, we chose several suitable PolSAR parameters and performed forest stem volume estimation using a non-parametric regression approach, to achieve improved performance compared to earlier studies.

The paper is organized as follows. In Section 2, the primary concepts of SAR polarimetry relevant for this study are provided, along with the description of specific PolSAR parameters that were examined. This sets the theoretic background of the study. Section 3 describes satellite SAR images and reference data, as well as specific methods used in the forest biomass estimation. Further, in Section 4, the primary analysis was performed and discussed. The study is concluded, indicating future research directions and potential, in Section 5.

2. Main PolSAR Concepts in the Context of the Study

Fully polarimetric measurement can be represented by a scattering matrix, essentially a linear mathematical operator describing transformation of incident electromagnetic wave into backscattered one:

$$[S] = \begin{bmatrix} S_{hh} & S_{hv} \\ S_{vh} & S_{vv} \end{bmatrix}. \tag{1}$$

where S_{pq} is the complex backscattering term associated with p transmit and q receive polarizations. In satellite borne SAR polarimetry, after polarimetric calibration and Faraday rotation compensation are performed (or in case latter is negligible), quad-polarimetric measurement for the

monostatic case can be represented by a lexicographic target vector $k_L = \left[S_{hh}, \sqrt{2} S_{hv}, S_{vv} \right]^T$. Second-order statistics of backscatter, suitable for describing polarimetric information content for complex and natural distributed targets, is obtained as an ensemble averaged outer product of the target vector k_L. The corresponding covariance matrix is positive semi-definite Hermittian:

$$[C3] = \begin{bmatrix} \langle S_{hh} S_{hh}^* \rangle & \langle \sqrt{2} S_{hh} S_{hv}^* \rangle & \langle S_{hh} S_{vv}^* \rangle \\ \langle \sqrt{2} S_{hv} S_{hh}^* \rangle & \langle 2 S_{hv} S_{hv}^* \rangle & \langle \sqrt{2} S_{hv} S_{vv}^* \rangle \\ \langle S_{vv} S_{hh}^* \rangle & \langle \sqrt{2} S_{vv} S_{hv}^* \rangle & \langle S_{vv} S_{vv}^* \rangle \end{bmatrix}. \tag{2}$$

This covariance matrix $[C3]$ (or equivalent coherence matrix $[T3]$ described further) can be used for characterizing a target via a change of polarization state of electromagnetic wave. Further, specific polarimetric observables can be further derived from it for ad hoc classification or characterization of the illuminated target.

Cloude and Pottier have proposed a polarimetric coherence matrix, reformulating the covariance matrix in the Pauli basis, with the target vector in reciprocal monostatic case given by $k = 1/\sqrt{2} \left[S_{hh} + S_{vv}, S_{hh} - S_{vv}, 2 S_{hv} \right]^T$ [45]. Then, the following expression is obtained:

$$[T3] = \frac{1}{2} \begin{bmatrix} \langle |S_{hh} + S_{vv}|^2 \rangle & \langle (S_{hh} + S_{vv})(S_{hh} - S_{vv})^* \rangle & \langle 2(S_{hh} + S_{vv}) S_{hv}^* \rangle \\ \langle (S_{hh} - S_{vv})(S_{hh} + S_{vv})^* \rangle & \langle |S_{hh} - S_{vv}|^2 \rangle & \langle 2(S_{hh} - S_{vv}) S_{hv}^* \rangle \\ \langle 2 S_{hv}(S_{hh} + S_{vv})^* \rangle & \langle 2 S_{hv}(S_{hh} - S_{vv})^* \rangle & 4 \langle |S_{hv}|^2 \rangle \end{bmatrix}. \tag{3}$$

Theory of target decomposition using eigenvalue or, alternatively, model based decomposition of coherence (or covariance) matrix has found wide application [12,46]. In this study, we will use several closely associated albeit different polarimetric measures based on the elements of coherence (or covariance) matrix.

The following PolSAR parameters are examined in the study:

- Backscattering coefficients (in dB) at HH, VV and HV polarizations. The corresponding expressions are given as

$$\sigma_{pq} = 10 * \log_{10} \left(\left\langle |S_{pq}|^2 \right\rangle \right). \tag{4}$$

- Total backscattered power (in dB), which can be calculated based on span of coherence/covariance matrix.

$$Span = trace([T3]) = trace([C3]); \quad P_t = 10 * \log_{10}(Span). \tag{5}$$

- Polarimetric coherence between two co-polarization channels. Both magnitude and phase are important here, as they provide degree of correlation and HH-VV phase difference.

$$\rho_{hhvv} = \left(\left\langle S_{hh} S_{vv}^* \right\rangle \middle/ \sqrt{\left\langle S_{hh} S_{hh}^* \right\rangle \left\langle S_{vv} S_{vv}^* \right\rangle} \right). \tag{6}$$

- Surface scattering fraction, given in [47] as

$$N_{11} = \frac{\left\langle |S_{hh} + S_{vv}|^2 \right\rangle}{\left\langle |S_{hh}|^2 \right\rangle + \left\langle |S_{vv}|^2 \right\rangle + 2 \left\langle |S_{hv}|^2 \right\rangle}. \tag{7}$$

- Even-bounce scattering fraction, which can be defined as a ratio:

$$N_{22} = \frac{\left\langle \left| S_{hh} - S_{vv} \right|^2 \right\rangle}{\left\langle \left| S_{hh} \right|^2 \right\rangle + \left\langle \left| S_{vv} \right|^2 \right\rangle + 2\left\langle \left| S_{hv} \right|^2 \right\rangle}. \tag{8}$$

Additionally, we use several more PolSAR parameters specifically formulated to capture vegetation characteristics, as follows:

- Radar Vegetation Index (RVI) given as

$$RVI = \frac{a\left\langle \left| S_{hv} \right|^2 \right\rangle}{\left\langle \left| S_{hh} \right|^2 \right\rangle + \left\langle \left| S_{vv} \right|^2 \right\rangle + 2\left\langle \left| S_{hv} \right|^2 \right\rangle}. \tag{9}$$

where typically a = 8, but can be adjusted to cover the dynamic range from 0 to 1. It was introduced in [48] with a goal of deriving a seasonally stable polarimetric descriptor for vegetated areas, but never really tested in forest biomass estimation. In forested terrain, it can be considered as a relative volume scattering contribution to the total backscattered power.

- Canopy Scattering Index defined as

$$CSI_{VV} = \frac{\left\langle \left| S_{vv} \right|^2 \right\rangle}{\left\langle \left| S_{hh} \right|^2 \right\rangle + \left\langle \left| S_{vv} \right|^2 \right\rangle}. \tag{10}$$

nd its modification (or supplement)

$$CSI_{HH} = \frac{\left\langle \left| S_{hh} \right|^2 \right\rangle}{\left\langle \left| S_{hh} \right|^2 \right\rangle + \left\langle \left| S_{vv} \right|^2 \right\rangle}. \tag{11}$$

The CSI parameter introduced in [49] is expected to provide sensitivity to forest variables as a measure of the relative importance of vertical against horizontal structure (or vice versa).

3. Data and Methods

Here, we first describe our study site, satellite SAR and ground reference data. Further, methodologies for forest stem volume estimation from individual PolSAR scenes are described, followed by SAR compositing approach and metrics for the accuracy assessment of retrieved stem volume estimates.

3.1. Study Site and In Situ Data

The study site is located in central Finland in vicinity of town Kuortane, with center coordinates: 62°49′N, 23°32′E (see Figure 1). The forest within the area is primarily mixed conifer-dominated, the main species being Scots pine (*Pinus sylvestris*), Norway spruce (*Picea abies*), and birch (*Betula pendula*, *Betula pubescens*). The primary soil type in the area is glacial drift, with occasional presence of well-drained sandy soils. The area is flat to hilly. Terrain elevation varies between 80 m and 130 m in the area of forest inventory data, and between 40 m and 226 m in the whole Digital Elevation Model (DEM) covered by the SAR images. The DEM obtained from the National Land Survey of Finland has a pixel spacing of 25 m and a vertical accuracy of about 2.5 m.
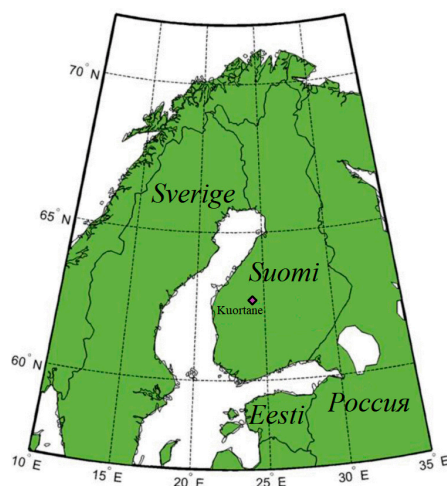
Figure 1. Study site location.

3.2. SAR Data

SAR data are represented by a time series of seven PolSAR scenes (see Figure 2) acquired during 2006–2009, at 24° incidence angle. Temperature and precipitation measurements from the nearby airport of Kauhava provide an indication of the local weather situation (Table 1). Majority of scenes were acquired in summer and leaf-on conditions, while two scenes were acquired under frozen conditions, and one during the snow melt.
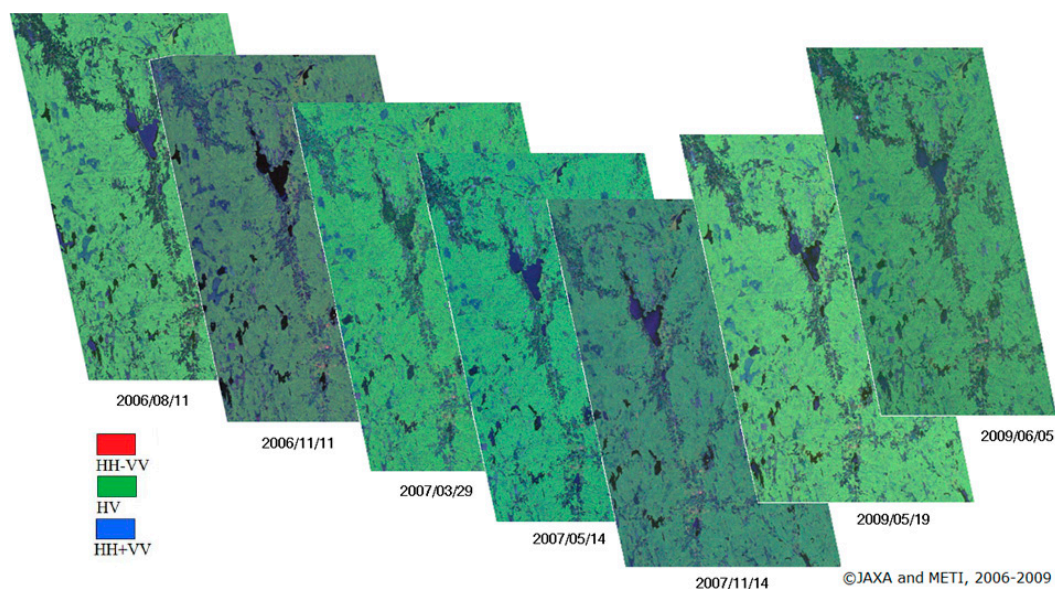

Figure 2. PolSAR time series acquired in 2006–2009, Pauli RGB color-composite representation.

Table 1. PolSAR scenes used in the study.

Acquisition Date	Temperature Mean (Min; Max), °C	Precipitation, mm
11 August 2006	18 (11; 26)	0.0
11 November 2006	−5 (−10; 0)	0.2
29 March 2007	6 (−1; 14)	0.0
5 May 2007	2 (−5; 10)	0.9
14 November 2007	−6 (−3; −9)	0.0
5 May 2009	8 (4; 11)	0.5
6 June 2009	6 (2; 9)	0.3

3.3. Reference Data

Reference data were represented by a stand-wise forest inventory made available by forest management companies in the study area. Only stands more than 2 ha were considered in the analysis to obtain more stable models. The overall number of stands was 124. The average stand size was 3.5 ha, median stand size was 3.2 ha and maximum was 6 ha. Stand-wise forest inventory data were updated to the year 2006. The forest inventory data were produced using standard methods for stand-wise inventory, primarily based on sample plots and visual interpretation. Forest stem volume varied between 0 and 314 m³/ha (area-weighted median 99 m³/ha, area-weighted mean 95 m³/ha). Locations of forest stands, along with the stem volume distribution, are shown in Figure 3.
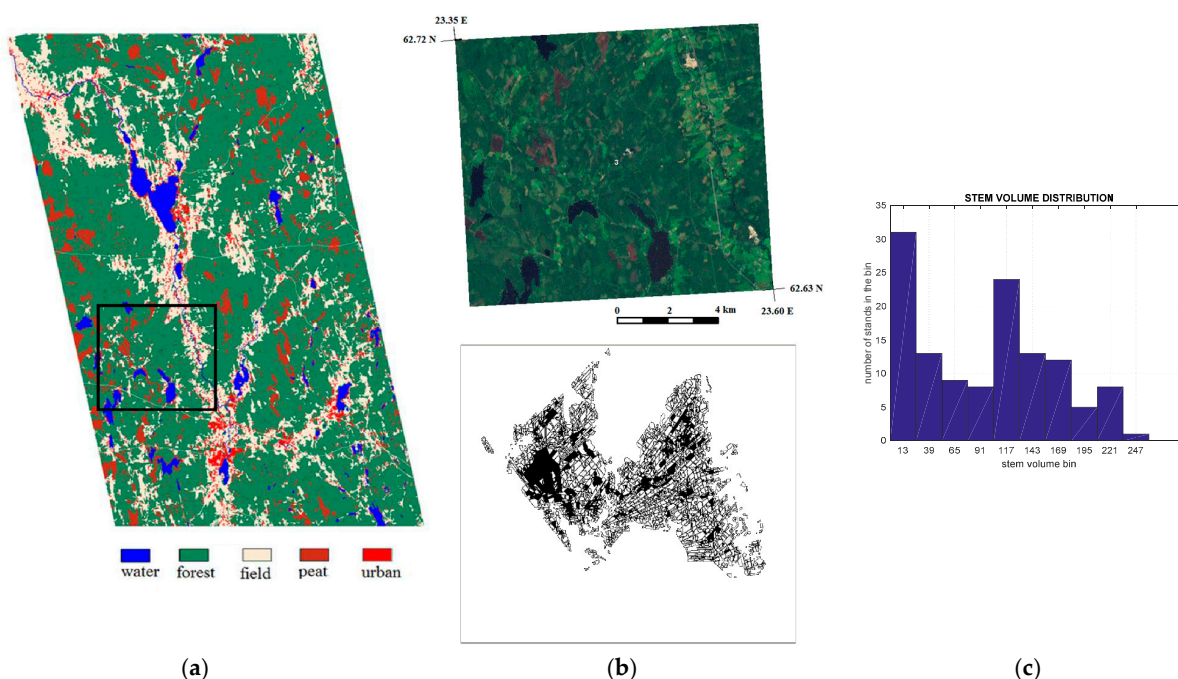

(**a**)　　　　　　　　　　　　　　　　(**b**)　　　　　　　　　　　　　　　　(**c**)

Figure 3. Reference data: (**a**) land cover in the study area; (**b**) forest inventory data location and mask of forest stands; (**c**) and forest stem volume distribution.

The forest stand mask was produced by rasterizing a forest inventory database provided by Etelä-Pohjanmaan Metsäkeskus (forest center). The stand mask was eroded by one pixel to avoid border effects in the processing. The forest stand mask overlaying SAR scene is shown in Figure 3 in the context of the reference land cover map.

For independent validation, the available dataset was divided for training and validation into two equal parts. To capture the whole dynamic range of forest stem volume and associated PolSAR parameters, the stands were arranged in descending order according to their stem volume and divided into two parts as odd or even numbers.

3.4. PolSAR Data Pre-Processing

The single look complex (SLC) level 1.1 PALSAR data were used for the investigations. The data were polarimetrically calibrated by JAXA as described in [50]. The pixel spacing of ortho-rectified scenes was set to 25 m. The DEMs were re-sampled to 25 m pixel spacing using cubic splines. Scenes were aggregated (averaged in the form of Stokes matrix elements over 6 consecutive image lines) in azimuth to obtain images with pixel dimensions approximately corresponding to the 25 m grid spacing. The images were ortho-rectified in the form of Stokes matrix data [51]. Bi-linear interpolation method was used for resampling in connection with the ortho-rectification. Radiometric normalization of intensity was done using a projected pixel area based approach [52], to minimize the effect of the topography. Correlation-derived tie points were used with the PolSAR image time series as the geo-location information was not precise enough. Map-derived ground control points

were used to revise the geo-location computed from the state vector and time code data in the ALOS PALSAR products.

Afterwards, the covariance/coherency matrix was formed, followed by speckle filtering (median filtering of 3 × 3). The estimate of the Faraday rotation angle [53,54] was within the 2° range indicating no expected influence on biophysical parameter retrieval [55].

To compensate for the slope effect, the polarization orientation angles (POAs) were derived from the circular polarization algorithm [56], as shown below:

$$\theta = \frac{1}{4}\left[\arctan\left(\frac{2\,\mathrm{Re}\{T_{23}\}}{T_{22} - T_{33}} \right) \right],$$ (12)

where θ is the phase difference between the right-right and left-left circular polarizations, and T_{pq} is a corresponding element of polarimetric coherence matrix. After the POA estimation, a new coherence matrix is formed using unitary line of sight rotation matrix:

$$[T3\_\theta] = [I\_\theta] * [T3] * [I\_\theta]^{-1},$$ (13)

With line of sight (LOS) matrix

$$[I\_\theta] = \begin{bmatrix} 1 & 0 & 0 \\ 0 & \cos 2\theta & \sin 2\theta \\ 0 & -\sin 2\theta & \cos 2\theta \end{bmatrix}.$$ (14)

All analysis was performed using stand-wise averaged SAR data. The averaged stand-wise values of elements of polarimetric covariance/coherence matrix were calculated in the power domain by averaging all pixel intensity values within each eroded stand (one-pixel erosion was applied).

3.5. SAR Based Estimation of Stem Volume

Forest stem volume was estimated based on two PolSAR parameters: cross-pol backscatter and co-pol coherence. Both parameters exhibit nonlinear dependence on biomass, with many suitable models available for their inversion [38,39,57].

In this study, due to presence of considerable reference data and to avoid peculiarities of, e.g., solving a system of two nonlinear equations, we used a non-parametric estimation technique: *k* nearest neighbor (kNN) regression method. Different nearest neighbor regression approaches became popular tools in estimating forest parameters from remotely sensed data [58–62]. Particularly, a multisource national forest inventory (NFI) in Finland is based on *k* nearest neighbor (kNN) approach [60,61]. Within the kNN regression methodology, the distance functions (between neighbors), number (*k*) of nearest neighbors and methods of their search, as well as weighting of the chosen neighbors, vary.

Here, we suggest estimating the forest stem volume of each stand as an average of forest stand values of the *k* nearest forest stands in the feature space of chosen PolSAR parameters. Here, we first describe measures and procedures needed for the kNN regression approach, and then proceed to the algorithm description.

Parameter *k*, the number of nearest neighbors, is an external parameter of the method. Distance between stands is calculated in the feature space of PolSAR parameters. Here, we chose *p* = 2 meaningful PolSAR parameters: HV backscatter and HHVV coherence. As their dynamic range varies, a linear stretching (standardization) was performed to have both coherence and backscatter within the [0; 1] dynamic range. In principle, such procedure is applicable also to other PolSAR parameters should they be chosen for predicting stem volume, such as e.g., RVI or various PolSAR ratios.

Distance *d* from evaluated stand *x* to reference stand *y* (in the feature space of dimensionality *p*), is, in general case, a Minkowski distance:

$$d = \left(\sum_{i=1}^{p} \left(|x_i - y_i| \right)^q \right)^{1/q}. \tag{15}$$

Here, we used $q = 2$, that is simply the Euclidean distance.

Finally, an estimate of the forest stem volume V_x^{est} was obtained as

$$V_x^{est} = (1/k) \sum_{y=1}^{k} V_y, \tag{16}$$

where x and y are forest stand indices, V_y is the stem volume of y-th nearest forest stand, and k is the number of nearest stands and the parameter of the kNN algorithm.

The idea of the kNN regression algorithm is schematically shown on the flowchart in Figure 4, and the algorithm proceeds as described in Algorithm 1.
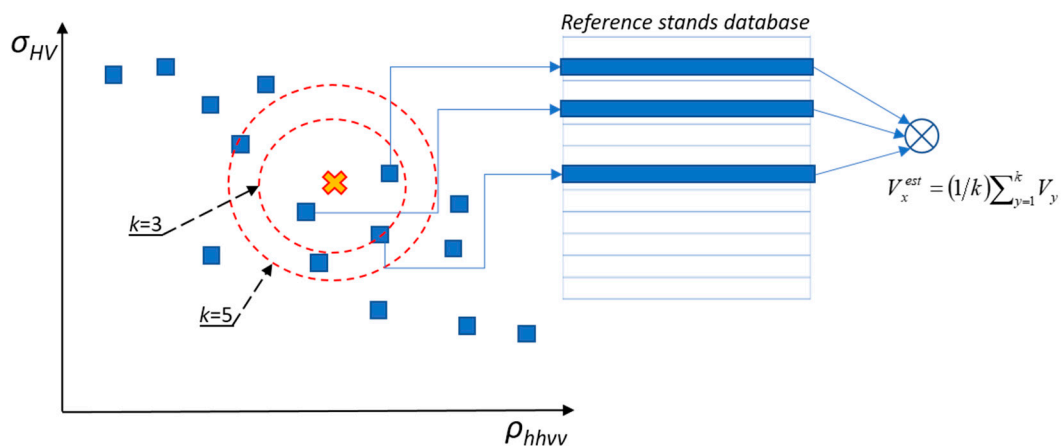

Figure 4. The conceptual scheme of the kNN regression approach.

The algorithm proceeds as follows:

Algorithm 1 kNN regression approach
1. Fix parameters of the algorithm (***k, p***)
2. Normalize/standardize the data in the feature space
3. For each forest stand, repeat: 　　a. Find its ***k*** nearest neighbors in the feature space. This requires: 　　　　i. Calculate pair-wise distances between the given stand and all reference stands using Equation (15), 　　　　ii. Arrange/rank reference stands in ascending order using calculated distances 　　b. Select ***k*** first reference stands, and supply their stem volume figures to (c). 　　c. Calculate an estimate of stand volume using Equation (16).

Parameter k was chosen within the range [2, N/2] where N is the number of training stands, based on the accuracy statistics calculated within the training dataset.

3.6. Multi-Scene Aggregation

To achieve better stability of the estimation, we used a multitemporal aggregation technique similar to those described in [63,64]. In the latter, Quegan and Yu have suggested a method for speckle filtering of SAR imagery by combining several channels or scenes. This approach is implemented as:

$$J_z(x,y) = \frac{\langle I_z(x,y) \rangle}{N} \sum_{i=1}^{N} \frac{I_i(x,y)}{\langle I_i(x,y) \rangle} \quad \text{with} \quad k = 1,...,N \tag{17}$$

where, at pixel position (x,y), $J_z(x,y)$ is the intensity of composite image (coherence matrix element), $I_i(x,y)$ is the intensity of *i*-th input image, $<I_i(x,y)>$ is the local average intensity of *i*-th input image, and N is the number of combined images.

Similar methodology is used here to combine PolSAR scenes in the intensity domain, before calculating PolSAR parameters of interest and performing stem-volume estimation. For each pixel location (x, y), each element of the coherence matrix is combined using Equation (17). We expect this approach to work best with images acquired in similar environmental conditions (where there is no bias caused by change of scattering mechanism due to, e.g., frozen state of forest or flooded terrain). Particular combinations of PolSAR scenes tested in the study, along with the results of the biomass estimation, are reported in Section 4.2.

3.7. Accuracy Analysis

Performance of the estimation approach was quantitatively evaluated using Root Mean Square Error (RMSE) as

$$RMSE = \sqrt{\frac{1}{N}\sum_{i=1}^{N}\left(V_i^{meas} - V_i^{est}\right)^2} , \qquad (18)$$

where N is the number of forest stands, and V_i^{meas} and V_i^{est} are measured and estimated values of forest stem volume for i-th stand, respectively. Further, relative RMSE was calculated by dividing absolute RMSE values by mean stem volume within the study site.

$$RMSE\ \% = \left(RMSE\ *\ N\right)\bigg/\left(\sum_{i=1}^{N}\left(V_i^{meas}\right)\right). \qquad (19)$$

In addition, the Pearson correlation coefficient *r* and coefficient of determination R^2 were used for interpretation, as traditionally adopted for this purpose in the remote sensing literature.

4. Results

Here, we first describe and discuss inter-dependencies between stand-wise estimates of different PolSAR parameters, as well as their relation to forest stem volume. Then, we chose two representative PolSAR parameters to predict the forest stem volume, namely co-polarization coherence and cross-polarization backscatter. Later, forest stem volume is estimated using the kNN method based on different combinations of these PolSAR parameters, as well as their multitemporal composites.

4.1. Temporal Dependence of PolSAR Parameters and Relation to Stem Volume

The PolSAR parameters presented earlier in Section 2 are analyzed here for each acquired scene. Figure 5 shows dependence of different PolSAR features as a function of forest stem volume. A scene acquired in August 2006 was chosen as a representative example. Here, most consistent monotonic behavior is demonstrated by HV-backscatter, RVI, co-polarization coherence magnitude and surface scattering fraction. As expected, the dependence is often nonlinear, increasing with saturation level for some parameters, and decreasing for others. Canopy scattering measure, instrumental in forest class differentiation, as a measure of the relative importance of vertical against horizontal structure (or vice versa), seems to be less adequate in capturing the stem volume dependence. Particularly, the CSI-HH version appears less suitable. Dependence for HH and VV backscatter on forest stem volume, and especially co-polarization coherence phase seems more "noisy" compared to other PolSAR parameters. For the latter, the reason can be forest understory, rich forest floor and presence of hilly terrain within the scenes; these factors make double bounce scattering mechanism due to ground–trunk interaction hindered. This is, however, in contrast to another polarimetric indicator, the relative even-bounce scattering mechanism, where clear dependence on the forest stem volume (albeit not as good as for HV-backscatter) is visible.

It is important to keep in mind that low correlation between forest stem volume and a specific PolSAR parameter does not necessarily suggest that the given parameter is suboptimal (e.g., for

further biomass retrieval), as the dependence can be nonlinear. In fact, Figure 5 clearly demonstrates that the assumption [11,26] on linear dependence between the forest stem volume and the majority of PolSAR parameters often fails; such approximation seems possible only over a certain range of the forest biomass values.
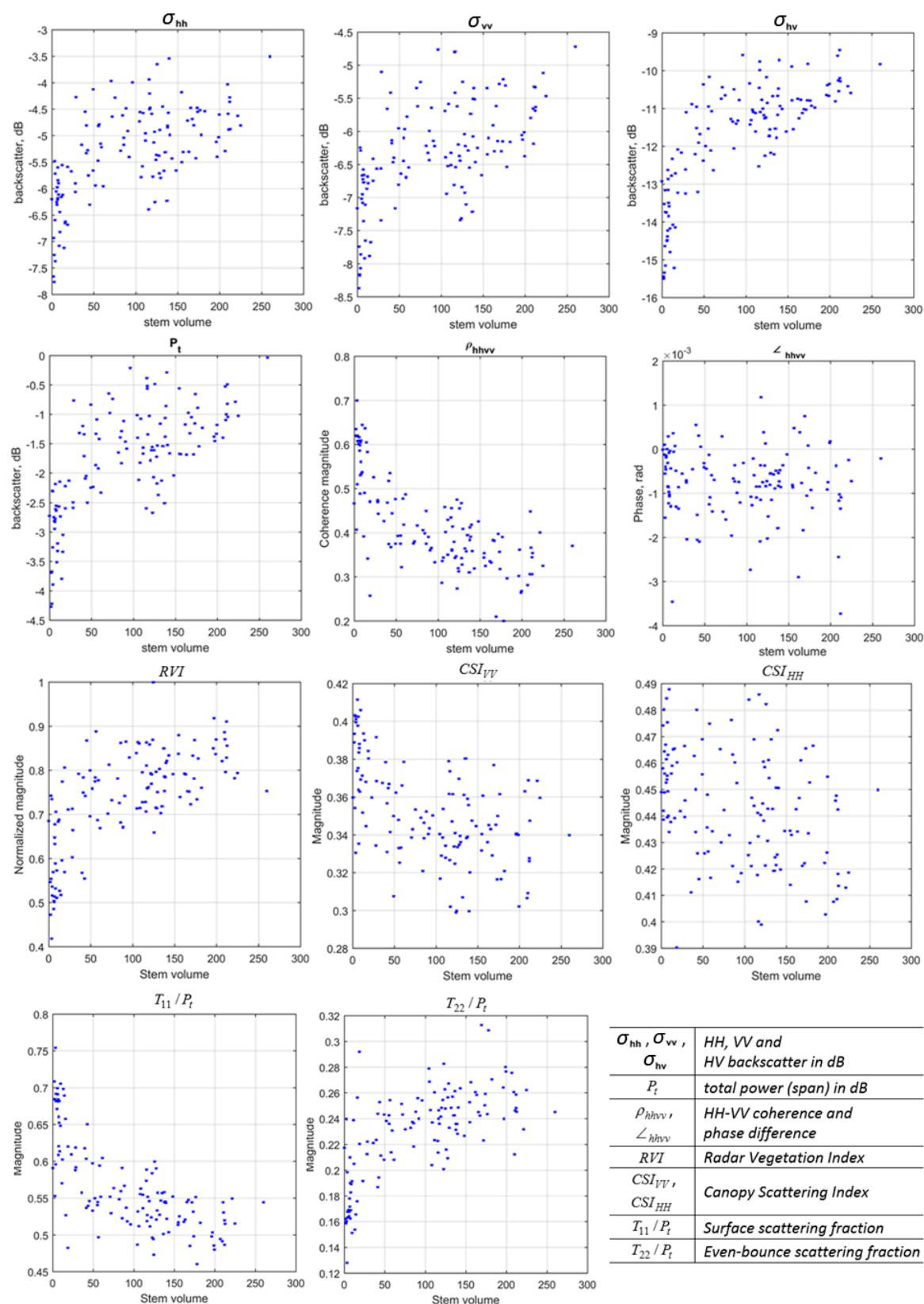

σ_{hh}, σ_{vv}, σ_{hv}	HH, VV and HV backscatter in dB
P_t	total power (span) in dB
ρ_{hhvv}, $\angle_{hhvv}$	HH-VV coherence and phase difference
RVI	Radar Vegetation Index
CSI_{VV}, CSI_{HH}	Canopy Scattering Index
T_{11}/P_t	Surface scattering fraction
T_{22}/P_t	Even-bounce scattering fraction

Figure 5. Dependence of PolSAR features on forest stem volume for selected scene (August 2006).

On the other hand, it is important to investigate the temporal dependence (or stability) of PolSAR parameters in relation to stem volume, as well as levels of correlation between different PolSAR parameters. The latter can help to seed out unnecessary (or unstable) parameters, while the former can suggest optimal conditions for the image acquisition, and hint on possible ways to aggregate different PolSAR scenes. As the Kuortane vicinities belong to intensively managed forest areas, it was easy to detect effects associated with clearcutting, particularly on the stand level. Several stands were detected as clear-cut especially within the last two-three scenes compared to other images, with the majority of PolSAR parameters being suitable to detect these changes. An example with cross-pol backscatter is shown in Figure 6. It is important to note that only non-cut stands (during the time span of 2006–2009) were used in calculating multitemporal statistics shown further, as well as in the forest stem volume retrieval.
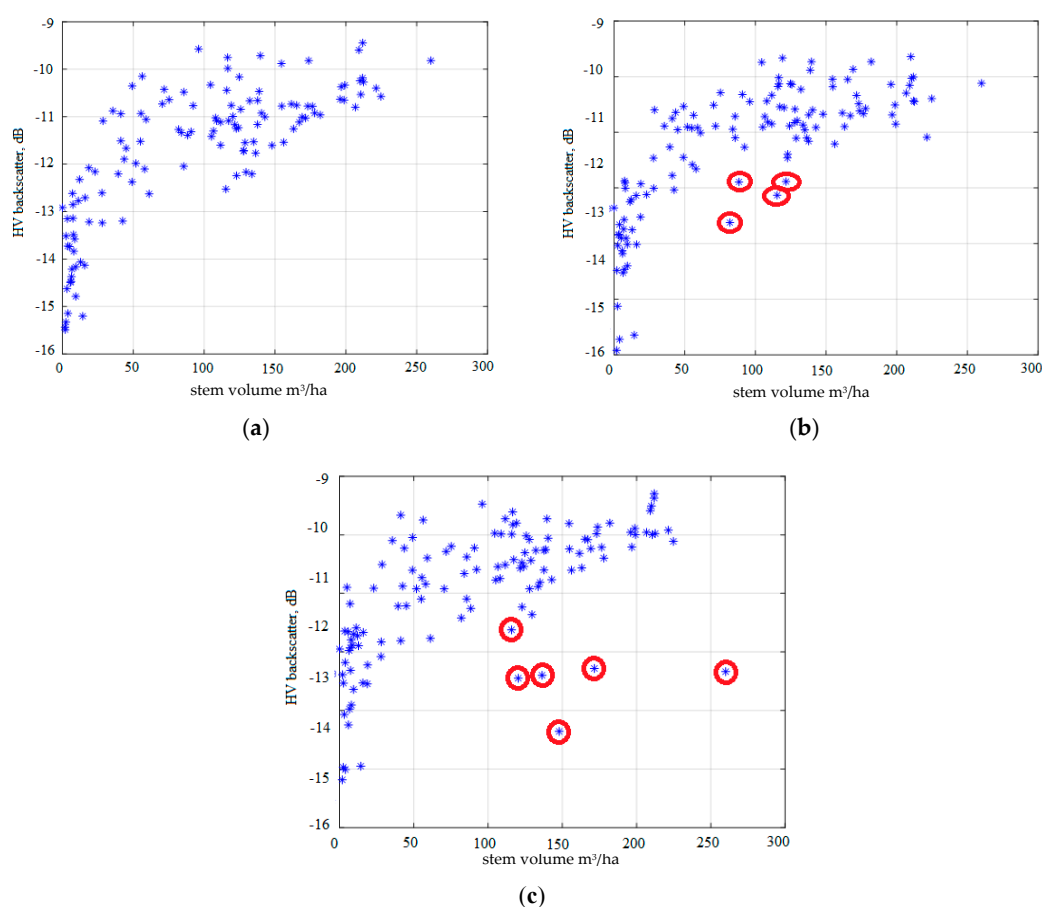

Figure 6. Temporal dynamics of cross-polarization backscatter reveals changes on stand level, with removal of at least six stands detected: (**a**) 11 August 2006; (**b**) 14 May 2007; and (**c**) 5 June 2009.

Figure 7 shows cross-correlation matrices for different PolSAR parameter in question, to assess the temporal stability between scenes. Another typical approach is to visualize these correlations explicitly as scatter-plots (e.g., as in [38]). In this situation, a level of 1 corresponds to fully linearly correlated dependence between corresponding two scenes (modulus of Pearson's correlation coefficient). Each pixel in respective correlation matrices corresponds to one scatterplot. As altogether there were seven ALOS PALSAR scenes, the correlation matrices for each PolSAR parameter have dimension 8 × 8 due to stem volume being included. To illustrate this approach in more detail, we show the 1st row of correlation matrix for σ_{hv} parameter as an ensemble of scatterplots in Figure 8. Here, even if a PolSAR parameter depends nonlinearly on stem volume, still high levels of correlation can indicate robustness of corresponding dependence (be it linear or nonlinear) across the seasons.
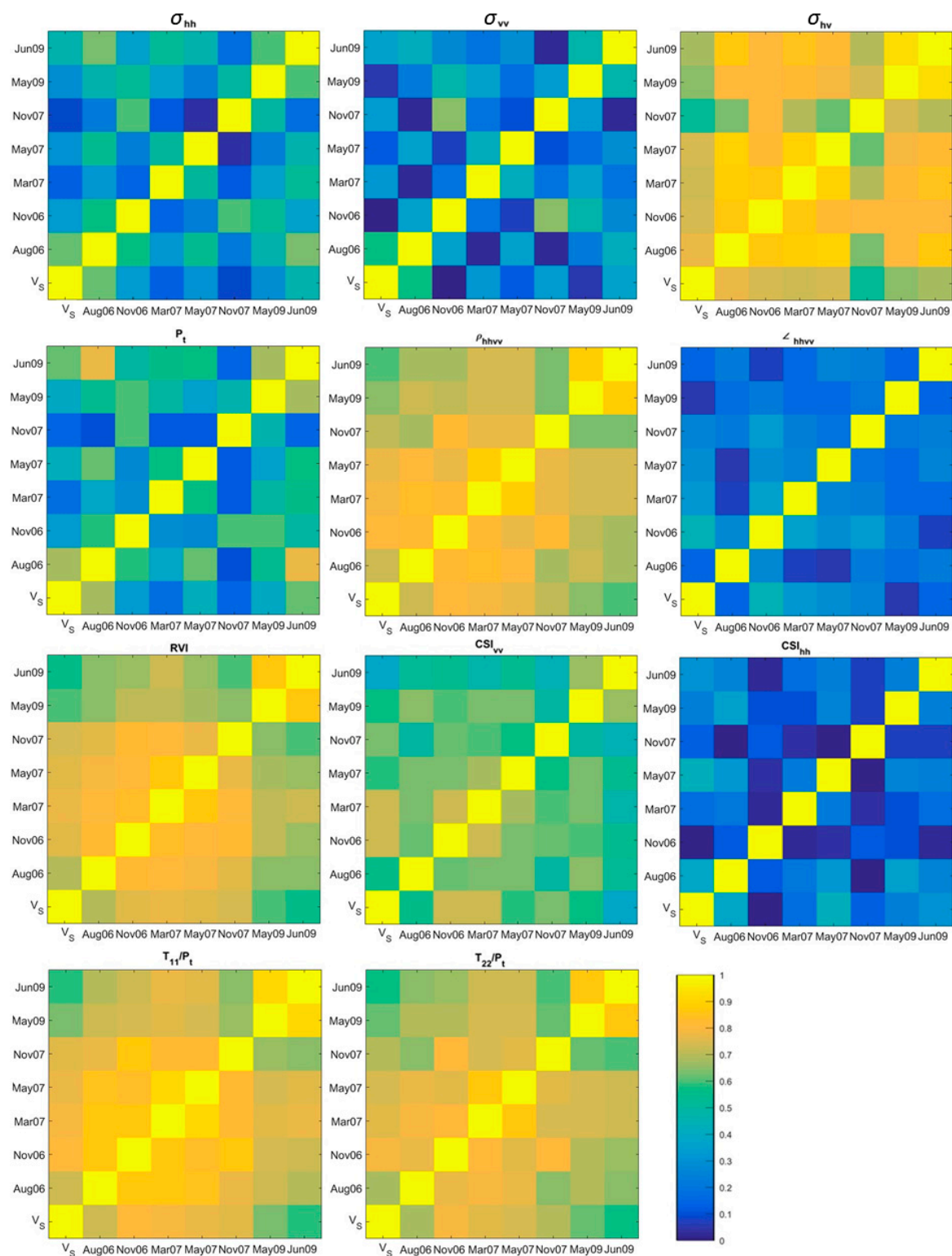
Figure 7. Correlation matrices illustrating levels of temporal correlation between stand-wise aggregates (averages) from different PolSAR scenes (for each studied PolSAR parameter), along with stem volume. As there were seven scenes, these correlation matrices have dimension 8 × 8.
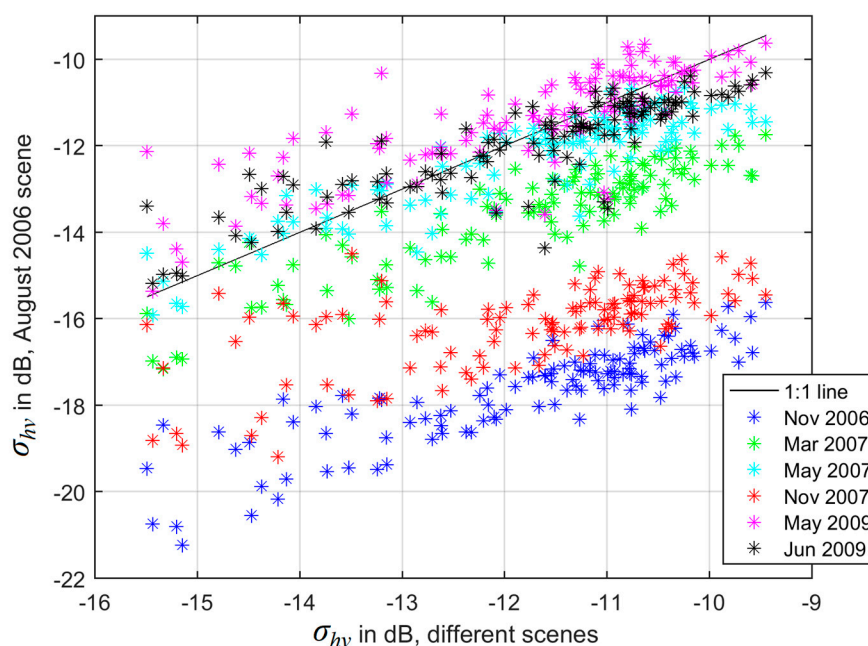
Figure 8. Scatterplots corresponding to the 1st (from the bottom) row of Correlation Matrix for HV-backscatter from Figure 7.

Most PolSAR parameters behave steadily across the time, though noticeable change occurs for November 2007 scene, as well as for two last scenes (stand-wise estimates of PolSAR parameters for which are highly correlated). In fact, it seems possible (most notably for RVI, polarimetric coherence and surface scattering fraction) to divide the time series into at least two groups: scenes acquired in 2006–2007 and scenes acquired in 2009. The reason for this dependence could be that the initial assumption on forest stem volume stability (for non-cut stands) starts to fail as we approach three-year difference between forest inventory and SAR measurements. This point is discussed further in Section 4. As far as specific PolSAR parameters are concerned, HH, VV and HH-VV phase as well as CSI-VV show low or modest levels of temporal cross-correlation, while other parameters seem to be quite stable.

In principle, a similar cross-correlation approach can be used to investigate interdependence between different PolSAR parameters (for each acquired scene), keeping in mind precautions about adequacy of such measure for nonlinear dependencies. Figure 9 shows linear cross-correlation matrices of different PolSAR parameters (as well as forest stem volume) for different PolSAR scenes.

Many PolSAR parameters exhibit high correlation to forest stem volume, as well as are correlated between themselves, and few exhibited good correlation also in temporal domain. Thus, it could be enough to choose only few representative parameters for further stem volume retrieval. One good candidate parameter is HV-backscatter widely used for assessment of forest biomass [65,66], as it is highly correlated to forest stem volume. Another representative PolSAR parameter we adopt is polarimetric coherence investigated in several earlier studies [42,43]. Another rationale for such choice is incorporating two PolSAR parameters with distinctly different dependence on stem volume, into the stem volume prediction. These two PolSAR parameters demonstrate different dynamics (both positive and negative correlation) as a function of forest stem volume. One more reason is that such combination (cross-polarization backscatter and co-polarization coherence) can be offered only by fully polarimetric SAR data, while assessment of such data potential is a primary concern of this study.
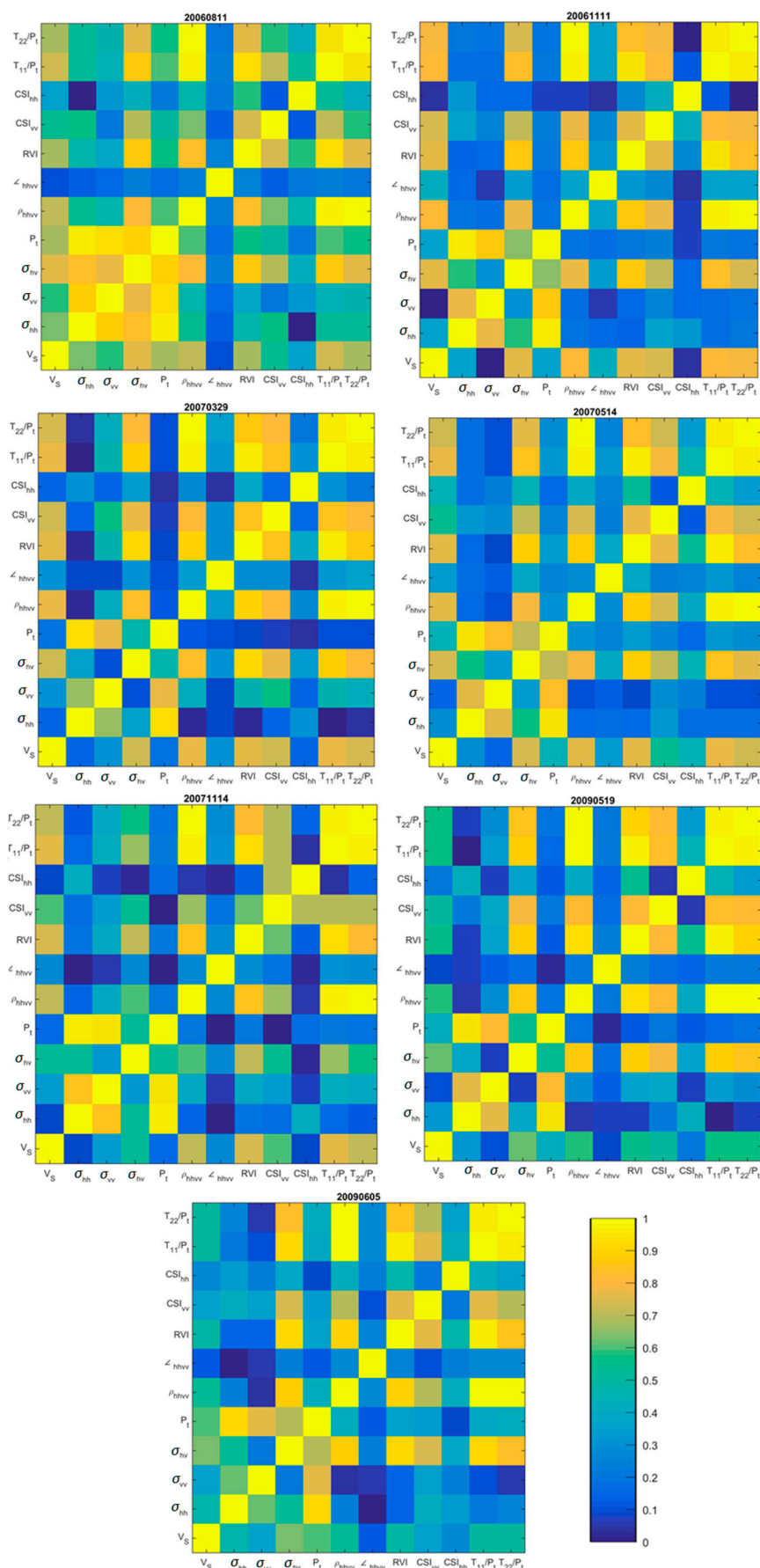
Figure 9. Correlation matrices illustrating how stand-wise estimates of PolSAR parameters are correlated to each other and to stem volume, for different acquisition dates (for each PolSAR scene). As there were altogether 11 PolSAR parameters, corresponding matrices have size 12 × 12.

4.2. Forest Stem Volume Estimation

Here, we estimate forest stem volume based on different combinations of two polarimetric parameters—cross-pol backscatter and co-pol coherence. To exclude temporal change effects, we have removed several stands (six altogether) where apparent change has happened during the observation time.

We use a non-parametric nearest neighbor technique for biomass estimation (described in Section 3.6), testing different scenarios of the PolSAR scene aggregation. As we had only seven scenes, an exhaustive search was used to find the best combinations in terms of RMSE. Other possible strategies for selecting scenes to be aggregated are discussed in Section 5.2. Interestingly, it was found better to aggregate four scenes for HV-backscatter, and five scenes for co-polarization coherence. One possible explanation is relatively high correlation between stem volume and co-polarization coherence of November 2008 scene (about the same as for previous four scenes), while HV-backscatter for the same scene has remarkably low correlation to stem volume.

Due to high correlation between the PolSAR scenes, effectiveness of multitemporal filtering was somewhat limited. Particularly, for the HV-backscatter (four scenes combined), the ENL increase factor was around 1.6–1.9 (times) compared to original scenes. Accuracy statistics for all scenes and parameters are collected in Table 2, with several notable results with best accuracies are highlighted. Scatterplots illustrating the best combinations are shown in Figure 10.

Polarimetric coherence for "winter" scenes was more suitable, with summer co-polarization coherence delivering generally worse accuracies. For HV-backscatter, scenes acquired over forests in "non-frozen" state were more suitable, as also supported by previous studies [5,7,42]. Overall, polarimetric coherence appeared to be a better predictor of the forest biomass for "frozen" scenes, as well as in winter conditions in the boreal zone (wet snow on March 2007 scene), while for other scenes the difference was quite marginal, aside from August 2006 scene (summer conditions) when the cross-pol backscatter performed better.

Table 2. Forest stem volume estimation with accuracy statistics.

| PolSAR Parameter	Scene	RMSE, m³ ha⁻¹	RMSE, %	r	R²	Notes
σ_{hv}	11 August 2006	41.0	43.2	0.81	0.66	
	11 November 2006	**40.8**	**42.9**	**0.81**	**0.66**	
	29 March 2007	44.6	46.9	0.77	0.59	
	14 May 2007	43.2	45.5	0.79	0.62	
	14 November 2007	56.4	59.1	0.59	0.35	
	19 May 2009	52.1	54.8	0.66	0.44	
	5 June 2009	49.7	52.3	0.70	0.49	
	multitemp	**39.1**	**41.2**	**0.83**	**0.69**	first 4 scenes combined
ρ_{hhvv}	11 August 2006	44.9	47.3	0.75	0.56	
	11 November 2006	38.8	40.8	0.84	0.71	
	29 March 2007	39.8	41.9	0.82	0.67	
	14 May 2007	42.6	44.8	0.80	0.64	
	14 November 2007	48.1	50.6	0.72	0.52	
	19 May 2009	47.7	50.2	0.74	0.55	
	5 June 2009	51.6	54.3	0.68	0.46	
	multitemp	**34.0**	**35.8**	**0.88**	**0.77**	first 5 scenes combined
σ_{hv} and ρ_{hhvv}	11 August 2006	40.7	42.8	0.82	0.67	
	11 November 2006	**37.4**	**39.4**	**0.85**	**0.72**	
	29 March 2007	**39.2**	**41.3**	**0.83**	**0.69**	
	14 May 2007	40.1	42.2	0.82	0.67	
	14 November 2007	45.9	48.3	0.75	0.56	
	19 May 2009	46.7	49.2	0.74	0.55	
	5 June 2009	49.2	51.8	0.70	0.49	
	multitemp	**32.2**	**33.9**	**0.89**	**0.79**	two multitemporal composites combined
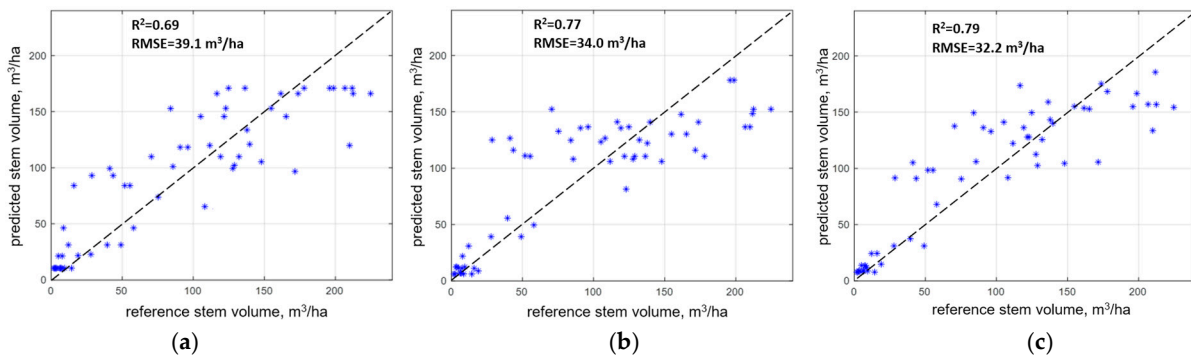
Figure 10. Scatterplots of ground-measured stem volume vs. stem volume retrieved from polarimetric parameters of combined ALOS PALSAR scenes: (**a**) σ_{hv} multitemp; (**b**) ρ_{hhvv} multitemp; and (**c**) σ_{hv} and ρ_{hhvv} multitemp.

On the other hand, practically for all scenes, combining two PolSAR parameters was useful. Notably, there were no scenes where combined parameters provided worse results than using any parameter separately. The improvement observed reached 5–6 m³/ha for separate scenes, though mostly it was relatively marginal. Implications, potential of combining PolSAR parameters and other relevant work are further discussed in Section 5.1. Considerable improvement was observed for selected multitemporal composites of the PolSAR scenes, with decreased RMSEs (up to 10–15 m³/ha) compared to the worst single-scene estimates. However, the improvement was relatively minor compared to the best estimates from single PolSAR scenes (2–5 m³/ha improvement). The best retrieved accuracy was on the order of 32 m³/ha and relative RMSE ≈ 34%. Peculiarities of multitemporal aggregation and possible strategies for selecting suitable scenes are further discussed in Section 5.2.

5. Discussion

5.1. Combining Polarimetric Coherence and Cross-Polarization Backscatter

In principle, this approach can be effectively implemented using one fully polarimetric scene (under suitable seasonal conditions), but multitemporal combination is preferable, as indicated by Table 2. In several earlier studies, it was noted that, in general, combining interferometric and intensity SAR data might be useful in estimating forest parameters. Particularly, in [57], the ERS InSAR data were combined with JERS-1 backscatter, and in [44,67], interferometric coherences of the ALOS PALSAR scenes acquired during winter were combined with summer backscatter intensities. The advantage of the approach explored in this study is that effective forest stem volume estimation can be performed from a separate/single PolSAR scene (unlike, e.g., SAR interferometry, where two scenes with suitable perpendicular and temporal baselines are needed). Here, we used a non-parametric approach that allowed avoiding explicit model training (though reference data were needed), in contrast to popular WCM (Water Cloud Model) based or semi-empirical parametric models often used in the forest biomass retrieval. Evaluating parametric approaches for PolSAR based biomass estimation using both polarimetric coherence and HV-backscatter, as well as use of ensemble learning methods (e.g., random forest regression in [68]) can be a further interesting extension of the study.

Other particularly promising PolSAR parameters were RVI and surface scattering fraction that demonstrated good stability in temporal analysis. This indicates potential towards use of them for robust forest parameter retrieval or forest stratification. Due to the orientation angle compensation of Equation (13), which is equivalent to minimizing the T_{33} term of the coherence matrix, an estimate of HV-backscatter can be considered conservative, with no contribution from slopes in the azimuth direction. As there are no major buildings (with walls non-parallel to the flight direction), or prominent rocks in the study area, no considerable cross-polarization scattering of oblique-dihedrals type is expected (which is a common reason for strong HV backscatter in urban areas). The incidence

angle was relatively steep, which could explain observed surface scattering sensitivity over forested areas. However, volume scattering dominates over both sparse and dense forested areas even with such incidence angle in "non-frozen" scenes, as explored in detail in our earlier study over Kuortane [15]. This was not the case under "frozen" conditions in November, when high levels of both volume and surface scattering were observed over sparsely forested areas. For larger incidence angles that are available from ALOS-2 PALSAR-2, we could expect larger sensitivity to volume scattering (and thus even better performance of HV-backscatter) and reduced contribution of backscattering from the ground. Comparing polarimetric signatures of ALOS PALSAR and ALOS-2 PALSAR-2 can constitute a potentially interesting extension of this study.

5.2. Multitemporal Aggregation and Forest Growth

It is important to keep in mind that the time series observation period was relatively long, and aside from abrupt changes such as clearcutting, a steady forest growth and biomass accumulation took place. In the study area, forest stem volume accumulates in the order of 4.7 m^3/ha per year [69]. This should affect early scenes less, as corresponding growth factors are quite small and can be accounted by introducing a small multiplier to stem volume figures. Particularly, for scenes acquired in 2006–2007 this factor can be neglected due to up to date forest inventory.

In multitemporal aggregation approaches over longer period, this can be a more crucial factor. It can be one of the reasons why stand-wise estimates of practically all PolSAR parameters from two last PolSAR scenes are highly correlated between themselves, and less correlated to a group of scenes acquired in 2006 and 2007. This indicates that temporal difference of 3–4 years in intensively managed boreal forest should be taken into consideration. Analysis of Table 2, however, reveals that even for summer 2009 scenes use of HV-backscatter as a predictor was providing much higher RMSEs, which can be attributed to accumulated forest growth during these three years (especially for regenerating stands with near-zero stem volume in the year 2006 according to the forest inventory).

Addressing optimality of the multitemporal scene aggregation is an important feature of the study. Here, the aggregation was performed for polarimetric coherence matrix element-wise, before calculating PolSAR features (such as polarimetric coherence). An important requirement for multichannel filtering of Quegan and Yu [64] is absence of bias [70]. While for HV-backscatter (which is also element T$_{33}$) the bias correction is straightforward, for PolSAR features that involve several elements of coherence matrix the bias correction is less trivial. The problem is that if different bias correction factors are applied to a given scene, it would alter scattering mechanism dependencies of the "corrected" stand-averaged coherence matrix. The importance of preserving polarimetric relationships within the coherence/covariance matrix is discussed in, e.g., Lee et al. [71] arguing that every polarimetric matrix element should be processed in the same manner to preserve statistical correlations between the polarimetric channels.

Alternatively, multitemporal aggregation could be implemented after calculating stand-wise PolSAR parameters for each separate scene. This can be followed by decorrelation (whitening) procedure of some kind, e.g., PCA [70]. One more approach, to avoid undesired bias due to seasonal conditions (such as flooded or frozen state of forests), could be including into the multitemporal averaging only scenes that are acquired under the same, optimal environmental conditions (verifying that scattering mechanisms are preserved in this way).

Here, due to presence of only seven scenes, we have performed an exhaustive search of optimal combination of scenes to achieve the best prediction of stem volume in terms of RMSE. Despite observed bias for the November 2006 scene, its presence was deemed optimal even without the bias correction, perhaps due to non-parametric nature of kNN. The reason could be also high correlation between stand-wise estimates of HV-backscatter and stem volume for this scene. That is, the presence of considerable bias did not disqualify the November 2006 scene. However, for another "frozen forest" scene (November 2007) we observed not only the bias (compared to August 2006) as shown in Figure 7, but also stronger variance (that is more poor precision).

It could indicate, that possible criterion for including a scene into the multitemporal averaging could be the level of correlation between the forest stem volume and considered PolSAR

scene/parameter on stand level. Such approach (maximizing the respective correlation at the forest stand level) was pursued in, (e.g., [34]). It seems suitable, however, when dependence between stem volume and PolSAR parameters is linear, which can be observed only for a limited range of stem volumes. However, another possible approach is to base the selection criteria on analysis of scatterplots such as shown in Figure 7. All scenes discarded from the multitemporal aggregation had high level of variance (low precision) compared to other scenes. Here, there also seems to be a trade-off between requirement of low variance between scenes (and thus higher correlation) and the fact that high correlation between scenes makes multitemporal filtering less effective. Apparently, not all of this variance can be simply explained by speckle (especially at stand level). Perhaps, different environmental conditions, changes in forest transmissivity, moisture and ground floor condition (and thus change of scattering mechanism) have a role to play.

Further benchmarking studies are needed to decide on the optimal multitemporal PolSAR data aggregation scenarios, where the goal is not only speckle reduction, but also optimal estimation of forest variables. Presently, such studies can be most easily organized using stacks of ESA Sentinel-1 dual-polarization data, as well as for ALOS PALSAR and ALOS-2 PALSAR-2 single/dual-polarization data, to have much higher number of studied scenes (tens to hundreds). It is also interesting to see if this approach is superior to another class of multitemporal approaches, where predicted forest variables from separate scenes are aggregated using multiple regression [37,39].

5.3. Relative Performance of Biomass Estimation Approach

Our results compare favorably to other spaceborne SAR studies at L-band over boreal forest. Most recent research on L-band SAR based forest biomass (AGB, growing stock volume, stem volume) estimation is well summarized in ([5], Table 3.1) and in ([6], Table 2). Among recent studies, in [40], the RMSE over natural taiga forest varied 25–32% of the mean biomass (R^2 in the range of 0.35–0.49); and, in [72], RMSE varied 31–46% of the mean biomass value and R^2 was 0.4–0.6 in forest stands in southern Sweden. The biomass prediction performance was also superior to earlier studies in Finnish boreal forest with multitemporal JERS-1 [11].

The area of Kuortane was studied also earlier using different types of EO (Earth Observation) data. Substantial improvement was achieved compared to our earlier study with dual-pol ALOS PALSAR data [39], when even multitemporal aggregation provided relatively moderate accuracy figures (RMSE of 43% and $R^2 = 0.61$). Comparison with earlier studies relying on satellite optical and other multisource data in [58,59] indicates advantage of suggested L-band PolSAR approach.

Multitemporal compositing approach in this study allowed improving stem volume prediction compared to single PolSAR scenes. It acted primarily on the SAR data level by reducing speckle as discussed above. There are also post-processing techniques that can contribute in improving the accuracy statistics: linear compositing of retrieved estimates based either on training with reference data (weights are assigned based on multiple regression) (as in, e.g., [37,39]), or SAR-derived metrics [38].

Adopted non-parametric kNN regression demonstrated relatively good performance. The limitation of this approach is, however, that predicted values of stem volume will always be within the dynamic range dictated by the training (ground reference) data. Thus, this approach is not suitable for extrapolation. If the training data are representative of expected stem volume variation, it seems safe to use the kNN regression method, as additionally evidenced by high levels of accuracies obtained in this study. Alternatively, parametric approaches as WCM with gaps [73], semi-empirical [36] and RVoG based models [74] can be recommended. Still widely used multivariate regression (as in, e.g., [11,75,76]) might be used as well, however care should be taken to linearize respective relationships [77]. Comparison of different biomass-retrieval methodologies was not pursued here as it was out of the study scope, and training data were representative enough.

6. Conclusions

We analyzed temporal behavior of several popular PolSAR parameters, as well as cross-correlation between these PolSAR parameters, and their relation to stem volume of boreal forests in

central Finland. As expected, many polarimetric parameters had similar behavior (nearly monotonically increasing with saturation for HV-backscatter, RVI, and even bounce scattering, and nearly monotonically decreasing for polarimetric coherence, CSI and even bounce scattering fraction), but levels of their correlation and temporal stability differed. Relation to forest stem volume was mostly nonlinear, suggesting that nonlinear parametric models as well as non-parametric approaches can provide better results in mapping forest variables.

Further, two representative PolSAR parameters, indicative of both positive and negative correlation to forest stem volume, namely cross-polarization backscatter and co-polarization coherence, were combined to provide an improved estimate compared to use of only one of these parameters. Overall, combining polarimetric coherence and cross-polarization backscatter with improved results in forest stem volume estimation for all PolSAR scenes, clearly indicates the advantage of a fully polarimetric mission over dual-polarization (provided other factors are the same and not considering resolution or swath width effects).

Results of multitemporal aggregation indicate that further, comprehensive effort might be needed to clearly formulate optimal aggregation strategies and criteria for including scenes into them. Feasible scenarios are selecting scenes based on similar environmental conditions during the SAR data takes, high levels of correlation between scenes and forest parameter of interest, low levels of variance between scenes, and absence of bias between scenes. The presence of bias was not important here due to nonparametric nature of the kNN approach. In parametric model based approaches, bias correction would be needed. Further research will be concentrated on improving parametric based inversion scenarios, to overcome problems with representativeness of reference data for the model training.

Author Contributions: O.A. designed the study and wrote the paper; Y.R. was involved in the data pre-processing; T.H. was primarily responsible for the satellite data acquisition and reference data provision; and J.P. was involved in the method development. All authors participated in the interpretation of the results and associated discussions, as well as revising the manuscript.

Conflicts of Interest: The authors declare no conflict of interest.

Abbreviations

AGB	Aboveground Biomass
ALOS	Advanced Land Observing Satellite
DEM	Digital Elevation Model
ESA	European Space Agency
ENL	Equivalent Number of Looks
EO	Earth Observation
InSAR	Interferometric Synthetic Aperture Radar
JAXA	Japanese Aero eXploration Agency
JERS	Japanese Earth Remote Sensing
NFI	National Forest Inventory
NN	Nearest Neighbors
PALSAR	Phased Array L-band Add-on SAR
POA	Polarization Orientation Angle
PolSAR	Polarimetric Synthetic Aperture Radar
RMSE	Root Mean Squared Error
RVoG	Random Volume over Ground
SAR	Synthetic Aperture Radar
SLC	Single Look Complex
WCM	Water Cloud Model

References

1. FAO. *Global Forest Resources Assessment 2005: Progress Towards Sustainable Forest Management*; FAO: Roma, Italy, 2006.
2. Saatchi, S.; Ulander, L.; Williams, M.; Quegan, S.; LeToan, T.; Shugart, H. Forest biomass and the science of inventory from space. *Nat. Clim. Chang.* **2012**, *2*, 826–827.
3. GCOS. *Status of the Global Observing System for Climate*; World Meteorological Organization: Geneva, Switzerland, 2015. Available online: https://library.wmo.int/pmb_ged/gcos_195_en.pdf (accessed on 1 July 2017).
4. Le Toan, T.; Quegan, S.; Woodward, I.; Lomas, M.; Delbart, N.; Picard, G. Relating radar remote sensing of biomass to modelling of forest carbon budgets. *Clim. Chang.* **2004**, *67*, 379–402.
5. Stelmaszczuk-Górska, M.A.; Thiel, C.J.; Schmullius, C.C. Remote sensing for aboveground biomass estimation in boreal forests. In *Earth Observation for Land and Emergency Monitoring*; Balzter, H., Ed.; Wiley: New York, NY, USA, 2017; 336 p.
6. Sinha, S.; Jeganathan, C.; Sharma, L.K.; Nathawat, M.S. A review of radar remote sensing for biomass estimation. *Int. J. Environ. Sci. Technol.* **2015**, *12*, 1779–1792.
7. Villard, L.; Le Toan, T.; TangMinh, D.H.; Mermoz, S.; Bouvet, A. Forest biomass from radar remote sensing. In *Land Surface Remote Sensing in Agriculture and Forest*; ISTE Press-Elsevier: London, UK, 2016; pp. 363–425.
8. Ouchi, K. Recent trend and advance of synthetic aperture radar with selected topics. *Remote Sens.* **2013**, *5*, 716–807.
9. Imhoff, M.L. Radar backscatter and biomass saturation: Ramifications for global biomass inventory. *IEEE Trans. Geosci. Remote Sens.* **1995**, *33*, 511–518.
10. Le Toan, T.; Beaudoin, A.; Riom, J.; Guyon, D. Relating forest biomass to SAR data. *IEEE Trans. Geosci. Remote Sens.* **1992**, *30*, 403–411.
11. Rauste, Y. Multi-temporal JERS SAR data in boreal forest biomass mapping. *Remote Sens. Environ.* **2005**, *97*, 263–275.
12. Cloude, S. *Polarisation: Applications in Remote Sensing*; Oxford University Press: Oxford, UK, 2009.
13. Riegger, S.; Werner, W. Wide-band polarimetric signatures as a basis for target classification. *Proc. IEEE* **1989**, *77*, 649–658.
14. Freeman, A; Durden, S.L. A three-component scattering model for polarimetric SAR data. *IEEE Trans. Geosci. Remote Sens.* **1997**, *36*, 963–973.
15. Antropov, O.; Rauste, Y.; Häme, T. Volume scattering modeling in PolSAR decompositions: Study of ALOS PALSAR data over boreal forest. *IEEE Trans. Geosci. Remote Sens.* **2011**, *49*, 3838–3848.
16. Xie, Q.; Ballester-Berman, J.D.; Lopez Sanchez, J.M.; Zhu, J.; Wang, C. On the use of generalized volume scattering models for the improvement of general polarimetric model-based decomposition. *Remote Sens.* **2017**, *9*, 117, doi:10.3390/rs90201017.
17. Green, R.M. Relationships between polarimetric SAR backscattering and forest canopy and sub-canopy biophysical properties. *Int. J. Remote Sens.* **1998**, *19*, 2395–2412.
18. Watanabe, M.; Shimada, M.; Rosenqvist, A.; Tadono, T.; Matsuoka, M.; Romshoo, S.A.; Ohta, K.; Furuta, R.; Nakamura, K.; Moriyama, T. Forest structure dependency of the relation between L-band and biophysical parameters. *IEEE Trans. Geosci. Remote Sens.* **2006**, *44*, 3154–3165.
19. Moghaddam, M. Analysis of scattering mechanisms in SAR imagery over boreal forest: Results from BOREAS'93. *IEEE Trans. Geosci. Remote Sens.* **1995**, *33*, 1290–1296.
20. Saatchi, S.S.; Moghaddam, M. Estimation of crown and stem water content and biomass of boreal forest using polarimetric SAR imagery. *IEEE Trans. Geosci. Remote Sens.* **2000**, *38*, 697–709.
21. Urbazaev, M.; Thiel, C.; Mathieu, R.; Naidoo, L.; Levick, S.R.; Smit, I.P.J.; Asner, G.P.; Schmullius, C. Assessment of the mapping of fractional woody cover in southern African savannas using multi-temporal and polarimetric ALOS PALSAR L-band images. *Remote Sens. Environ.* **2015**, *166*, 138–153.
22. Maghsoudi, Y.; Collins, M.; Leckie, D.G. Polarimetric classification of boreal forest using nonparametric feature selection and multiple classifiers. *Int. J. Appl. Earth Obs. Geoinf.* **2012**, *19*, 139–150.
23. Antropov, O.; Rauste, Y.; Astola, H.; Praks, J.; Häme, T.; Hallikainen, M.T. Land cover and soil type mapping from spaceborne PolSAR data at L-band with probabilistic neural network. *IEEE Trans. Geosci. Remote Sens.* **2014**, *52*, 5256–5270.
24. Antropov, O.; Rauste, Y.; Lönnqvist, A.; Häme, T. PolSAR mosaic normalization for improved land-cover mapping. *IEEE Geosci. Remote Sens. Lett.* **2012**, *9*, 1074–1078.

25. Karam, M.A.; Amar, F.; Fung, A.K.; Mougin, E.; Lopes, A.; Le Vine, D.M.; Beaudoin, A. A microwave polarimetric scattering model for forest canopies based on vector radiative transfer theory. *Remote Sens. Environ.* **1995**, *53*, 16–30.

26. Balzter H.; Baker, J.R.; Hallikainen, M.; Tomppo, E. Retrieval of timber volume and snow water equivalent over a Finnish boreal forest from airborne polarimetric synthetic aperture radar. *Int. J. Remote Sens.* **2002**, *23*, 3185–3208.

27. Proisy, C.; Mougin, E.; Fromard, F.; Karam, M.A. Interpretation of polarimetric radar signatures of mangrove forests. *Remote Sens. Environ.* **2000**, *71*, 56–66.

28. Hoekman, D.H.; Quinones, M.J. Land cover type and biomass classification using AirSAR data for evaluation of monitoring scenarios in the Colombian Amazon. *IEEE Trans. Geosci. Remote Sens.* **2000**, *38*, 685–696.

29. Garestier, F.; Dubois-Fernandez, P.C.; Guyon, D.; Le Toan, T. Forest biophysical parameter estimation using L- and P-band polarimetric SAR data. *IEEE Trans. Geosci. Remote Sens.* **2009**, *47*, 3379–3388.

30. Gonçalves, F.G.; Santos, J.R.; Treuhaft, R.N. Stem volume of tropical forests from polarimetric radar. *Int. J. Remote Sens.* **2011**, *32*, 503–522.

31. Praks, J.; Alasalmi, H.; Hallikainen, M. Polarimetric properties of boreal forest in L- and C-band SAR images. In Proceedings of the IEEE 2001 International Geoscience and Remote Sensing Symposium, Sydney, Australia, 9–13 July 2001; pp. 3050–3052.

32. Rauste, Y.; Hame, T.; Pullianen, J.; Heiska, K.; Hallikainen, M. Radar-based forest biomass estimation. *Int. J. Remote Sens.* **1994**, *15*, 2797–2808.

33. Rauste, Y.; Lönnqvist, A.; Ahola, H. Mapping boreal forest biomass with imagery from polarimetric and semi-polarimetric SAR sensors. *Ambiencia* **2008**, *4*, 171–180.

34. Neumann, M; Saatchi, S. Polarimetric backscatter optimization for biophysical parameter estimation. *IEEE Geosci. Remote Sens. Lett.* **2014**, *11*, 254–258.

35. Rosenqvist, Å.; Shimada, M.; Ito, N.; Watanabe, M. ALOS PALSAR: A pathfinder mission for global-scale monitoring of the environment. *IEEE Trans. Geosci. Remote Sens.* **2007**, *45*, 3307–3316.

36. Pulliainen, J.T.; Kurvonen L.; Hallikainen M.T. Multitemporal behavior of L- and C-band SAR observations of boreal forests. *IEEE Trans. Geosci. Remote Sens.* **1999**, *37*, 927–937.

37. Kurvonen, L.; Pulliainen, J.; Hallikainen, M. Retrieval of biomass in boreal forests from multitemporal ERS-1 and JERS-1 SAR images. *IEEE Trans. Geosci. Remote Sens.* **1999**, *37*, 198–205.

38. Santoro, M.; Eriksson, L.E.B.; Fransson, J.E.S. Reviewing ALOS PALSAR backscatter observations for stem volume retrieval in Swedish forest. *Remote Sens.* **2015**, *7*, 4290–4317.

39. Antropov, O.; Rauste, Y.; Ahola, H.; Häme, T. Stand-level stem-volume of boreal forests from spaceborne SAR imagery at L-band. *IEEE J. Sel. Top. Appl. Earth Obs. Remote Sens.* **2013**, *10*, 142–149.

40. Peregon, A.; Yamagata, Y. The use of ALOS/PALSAR backscatter to estimate above-ground forest biomass: A case study in Western Siberia. *Remote Sens. Environ.* **2013**, *137*, 139–146.

41. Cartus, O.; Santoro, M.; Kellndorfer, J. Mapping forest aboveground biomass in the Northeastern United States with ALOS PALSAR dual polarization L-band. *Remote Sens. Environ.* **2012**, *124*, 466–478.

42. Chowdhury, T.A.; Thiel, C.; Schmullius, C. Growing stock volume estimation from L-band ALOS PALSAR polarimetric coherence in Siberian forest. *Remote Sens. Environ.* **2014**, *155*, 129–144.

43. Chowdhury, T.A.; Thiel, C.; Schmullius, C.; Stelmaszczuk-Górska, M. Polarimetric parameters for growing stock volume estimation using ALOS PALSAR L-Band data over Siberian forests. *Remote Sens.* **2013**, *5*, 5725–5756.

44. Thiel, C; Schmullius, C. The potential of ALOS PALSAR backscatter and InSAR coherence for forest growing stock volume estimation in Central Siberia. *Remote Sens. Environ.* **2016**, *173*, 258–273.

45. Cloude, S.R.; Pottier, E. A review of target decomposition theorems in radar polarimetry. *IEEE Trans. Geosci. Remote Sens.* **1996**, *34*, 498–518.

46. Richards, J.A. *Remote Sensing with Imaging Radar*; Springer: Berlin/Heidelberg, Germany, 2009.

47. Praks, J.; Koeniguer, E.; Hallikainen, M.T. Alternatives to target entropy and alpha angle in SAR polarimetry. *IEEE Trans. Geoci. Remote Sens.* **2009**, *47*, 2262–2274.

48. Kim, Y.; Van Zyl, J. Comparison of forest parameter estimation techniques using SAR data. In Proceedings of the IEEE 2001 International Geoscience and Remote Sensing Symposium, Sydney, Australia, 9–13 July 2001; pp. 1395–1397.

49. Pope, K.O.; Rey-Benayas, J.M.; Paris, J.F. Radar remote sensing of forest and wetland ecosystems in the Central American tropics. *Remote Sens. Environ.* **1994**, *48*, 205–219.

50. Shimada, M.; Isoguchi, O.; Tadono, T.; Isono, K. PALSAR radiometric and geometric calibration. *IEEE Trans. Geosci. Remote Sens*. **2009**, *47*, 3915–3932.

51. Rauste, Y.; Lönnqvist, A.; Molinier, M.; Henry, J-B.; Häme, T. Ortho-rectification and terrain correction of polarimetric SAR data applied in the ALOS/Palsar context. In Proceedings of IEEE International Geoscience and Remote Sensing Symposium, Barcelona, Spain, 23–27 July 2007; pp. 1618–1621.

52. Small, D. Flattening gamma: Radiometric terrain correction for SAR imagery. *IEEE Trans. Geosci. Remote Sens*. **2011**, *49*, 3081–3093.

53. Freeman, A. Calibration of linearly polarized polarimetric SAR data subject to Faraday rotation. *IEEE Trans. Geosci. Remote Sens*. **2004**, *42*, 1617–1624.

54. Sandberg, G.; Eriksson, L.E.B.; Ulander, L.M.H. Measurements of Faraday rotation using polarimetric PALSAR images. *IEEE Geosci. Remote Sens. Lett*. **2009**, *6*, 142–146.

55. Freeman, A.; Saatchi, S.S. On the detection of Faraday rotation in linearly polarized L-band SAR backscatter signatures. *IEEE Trans. Geosci. Remote Sens*. **2004**, *42*, 1607–1616.

56. Lee, J.S.; Ainsworth, T.L. The effect of orientation angle compensation on coherency matrix and polarimetric target decomposition. *IEEE Trans. Geosci. Remote Sens*. **2011**, *49*, 53–64.

57. Wagner, W.; Luckman, A.; Vietmeier, J.; Tansey, K.; Balzter, H.; Schmullius, C.; Davidson, M.; Gaveau, D.; Gluck, M.; Le Toan, T.; et al. Large-scale mapping of boreal forest in SIBERIA using ERS tandem coherence and JERS backscatter data. *Remote Sens. Environ*. **2003**, *85*, 125–144.

58. Packalen, P; Maltamo, M. The k-MSN method in the prediction of species specific stand attributes using airborne laser scanning and aerial photographs. *Remote Sens. Environ*. **2007**, *109*, 328–341.

59. Maltamo, M; Packalen, P.; Suvanto, A; Korhonen, K.T.; Mehtätalo, L.; Hyvönen, P. Combining ALS and NFI training data for forest management planning: A case study in Kuortane, Western Finland. *Eur. J. Forest Res.* **2009**, *128*, 305–317.

60. Tomppo, E. The Finnish multi-source National Forest Inventory—Small area estimation and map production. In *Forest Inventory: Methodology and Applications. Managing Forest Ecosystems*; Kangas, A., Maltamo, M., Eds.; Springer: Dordrecht, The Nederlands, 2006; pp. 195–224.

61. Tomppo, E.; Halme, M. Using coarse scale forest variables as ancillary information and weighting of variables in k-NN estimation: A genetic algorithm approach. *Remote Sens. Environ*. **2004**, *92*, 1–20.

62. Finley, A.O.; McRoberts, R.E.; Ek, A.R. Applying an efficient k nearest neighbor search to forest attribute imputation. *Forest Sci*. **2006**, *52*, 130–135.

63. Quegan, S.; Le Toan, T.; Yu, J.J.; Ribbes, F.; Floury, N. Multitemporal ERS SAR analysis applied to forest mapping. *IEEE Trans. Geosci. Remote Sens*. **2000**, *38*, 741–753.

64. Quegan, S.; Yu, J.J. Filtering of multichannel SAR images. *IEEE Trans. Geosci. Remote Sens*. **2001**, *39*, 2373–2379.

65. Dobson, M.C.; Ulaby, F.T.; Le Toan, T.; Beaudoin, A.; Kasischke, E.S.; Christensen, N. Dependence of radar backscatter on coniferous forest biomass. *IEEE Trans. Geosci. Remote Sens*. **1992**, *30*, 412–415.

66. Ranson, K.J.; Sun, G. Mapping biomass of a northern forest using multifrequency SAR data. *IEEE Trans. Geosci. Remote Sens*. **1994**, *32*, 388–396.

67. Thiel, C.J.; Thiel, C.; Schmullius, C.C. Operational large-area forest monitoring in Siberia using ALOS PALSAR summer intensities and winter coherence. *IEEE Trans. Geosci. Remote Sens*. **2009**, *47*, 3993–4000.

68. Baghdadi, N.; Le Maire, G.; Bailly, J.S.; Osé, K.; Nouvellon, Y.; Zribi, M.; Lemos, C.; Hakamada, R. Evaluation of ALOS/PALSAR L-band data for the estimation of Eucalyptus plantations aboveground biomass in Brazil. *IEEE J. Sel. Top. Appl. Earth Obs. Remote Sens*. **2015**, *8*, 3802–3811.

69. Finnish Forest Research Institute. *Finnish Statistical Yearbook of Forestry, 2012*; Finnish Forest Research Institute: Vantaa, Finland, 2012; p. 71.

70. Oliver, C.; Quegan, S. *Understanding Synthetic Aperture Radar Images*; SciTech Publishing: Raleigh, NC, USA, 2004.

71. Lee, J.-S.; Grunes, M.R.; Schuler, D.L.; Pottier, E.; Ferro-Famil, L. Scattering-model-based speckle filtering of polarimetric SAR data. *IEEE Trans. Geosci. Remote Sens*. **2006**, *44*, 176–187.

72. Sandberg, G.; Ulander, L.M.H.; Fransson, J.E.S.; Holmgres, J.; Le Toan, T. L- and P-band backscatter intensity for biomass retrieval in hemiboreal forest. *Remote Sens. Environ*. **2011**, *115*, 2874–2886.

73. Askne, J.; Santoro, M.; Smith, G.; Fransson, J.E.S. Multitemporal repeat-pass SAR interferometry of boreal forests. *IEEE Trans. Geosci. Remote Sens*. **2003**, *41*, 1540–1550.

74. Olesk, A.; Praks, J.; Antropov, O.; Zalite, K.; Arumäe, T.; Voormansik, K. Interferometric SAR Coherence Models for Characterization of Hemiboreal Forests Using TanDEM-X Data. *Remote Sens*. **2016**, *8*, 700, doi:10.3390/rs8090700.

75. Englhart, S.; Keuck, V.; Siegert, F. Modeling aboveground biomass in tropical forests using multi-frequency SAR data—A comparison of methods. *IEEE J. Sel. Top. Appl. Earth Obs. Remote Sens*. **2012**, *5*, 298–306.

76. Hyyppä, J.; Hyyppä, H.; Inkinen, M.; Engdahl, M.; Linko, S.; Zhu, Y.-H. Accuracy comparison of various remote sensing data sources in the retrieval of forest stand attributes. *Forest Ecol. Manag.* **2000**, *128*, 109–120.

77. Hame, T.; Rauste, Y.; Antropov, O.; Ahola, H.A.; Kilpi, J. Improved mapping of tropical forests with optical and SAR imagery, Part II: Above ground biomass estimation. *IEEE J. Sel. Top. Appl. Earth Obs. Remote Sens.* **2013**, *6*, 92–101.